

Stability conditions and Fermi surface topologies in a superconductor

Elena Gubankova,^{1,*} Andreas Schmitt,^{1,2,†} and Frank Wilczek^{1,‡}

¹*Center for Theoretical Physics, Massachusetts Institute of Technology, Cambridge, MA 02139, USA*

²*Department of Physics, Washington University St Louis, MO, 63130, USA*

(Dated: March 23, 2022)

Candidate homogeneous, isotropic superfluid or superconducting states of paired fermion species with different chemical potentials, can lead to quasiparticle excitation energies that vanish at either zero, one, or two spheres in momentum space. With no zeroes, we have a conventional BCS superconductor. The other two cases, “gapless” superconductors, appear in mean field theory for sufficiently large mismatches and/or sufficiently large coupling strengths. Here we examine several stability criteria for those candidate phases. Positivity of number susceptibility appears to provide the most powerful constraint, and renders all the two-zero states that we have examined mechanically unstable. Our results should apply directly to ultracold fermionic atom systems.

PACS numbers: 03.75.Ss, 11.15.Ex

I. INTRODUCTION

In a conventional superconductor the Fermi surface disappears [1]. Anisotropic fermion pairing is known, in several cases, to leave behind residual lower-dimensional effective Fermi surfaces: excitations of infinitesimal energy exist only in certain directions, defined by isolated points or lines in momentum space. This situation occurs for instance in the *A* phase of helium-3 [2], in high-temperature superconductors [3] or in certain phases in color-superconducting quark matter [4].

It has been suggested that isotropic multi-fermion systems with attraction between species that have Fermi surfaces of different size could lead to a more extreme version of this phenomenon, wherein pairing and superfluidity could coexist with gapless excitations across entire spheres. Indeed, there is competition between the possibility to lower the energy by pairing one-particle states of equal and opposite momenta (\mathbf{p} , $-\mathbf{p}$) coherently [1], to take advantage of the favorable interaction energy, and the fact that minimizing the kinetic energy does not put low-energy states at such momenta. Thus plausibly it might become favorable to move fermions into different momentum states before pairing, taking a hit in kinetic energy, in order to profit from interaction energy. Depending on where the excess fermions stayed, since it was too costly to move them, and on the extent of the superfluid gap, “scars”, in the form of discontinuities in the occupation number, could be left behind. Such scars appear as residual Fermi surfaces.

If the mismatch is small and the gap is large, any scars are covered over. In that case the two fermion species have equal number densities and the superfluid state does not support gapless single-particle excitations. If it is appropriate to think that fermions of one species adjust

to the other, e.g. by promoting fermions from the top of the smaller Fermi surface to match the larger Fermi surface and leaving the distribution with larger Fermi surface almost untouched, then one free Fermi surface is left behind. This phase was proposed at large particle number asymmetry and strong coupling [5]. Here, the entire remaining Fermi sphere is occupied by unpaired particles of one species. If it is appropriate to think that the compromise is reached by moving some fermions up from the smaller Fermi surface and others down from the larger Fermi surface while leaving unpaired fermions in between, then two free surfaces are left behind. This has been termed the “breached” proposal [6]. (In the literature the terminology is not entirely uniform, but this usage seems appropriate and convenient.) At large mass ratio, the dominant pairing comes from the interior region [7].

In a system with Fermi surface mismatch and *p*-wave pairing, the effective residual Fermi surface can assume complicated two-dimensional shapes, e.g., topologically equivalent to a torus [8]. In this paper, however, we consider only isotropic effective masses and interactions, and s-wave pairing.

Before describing the technical content of this paper, let us mention two concrete physical systems in which these unconventional superconducting or superfluid states are expected and possibly already observed.

Remarkable control has been achieved over systems of ultracold fermionic atoms. Many important parameters such as the number densities and the coupling strength can be varied. These systems are studied in optical traps where an external magnetic field provides the “knob” to control the coupling strength around a Feshbach resonance [9]. By choosing different magnetic fields, the crossover from the BCS to the Bose-Einstein condensed (BEC) region can be observed. For theoretical studies on this crossover see for instance [10]. Recently experimental studies have been extended to systems of atoms in two different spin states with mismatched number densities [11]. What was a crossover in the symmetric situation then appears to resolve into one or more phase

*Electronic address: elena1@mit.edu

†Electronic address: aschmitt@wuphys.wustl.edu

‡Electronic address: wilczek@mit.edu

transitions. For some values of the mismatch and the coupling, the results seem to suggest a mixed phase, i.e., a coexistence of spatially separated superfluid and normal phases [12], as predicted in Ref. [13].

Another example for unconventional superconductivity is quark matter in the interior of neutron stars. If sufficiently cold and dense, this matter is color-superconducting [14, 15]. Quark matter can, in principle, form Cooper pairs in many different patterns. At asymptotically high densities, where the quark masses can be neglected, the highly symmetric and fully gapped color-flavor locked (CFL) phase [16] is favored. At intermediate densities, many more pairing patterns are thinkable. All of them involve pairing of quarks with different Fermi surfaces [17]. Gapless phases are conceivable, though the question of the true ground state is currently unsolved. While in this paper we focus on nonrelativistic two-fermion systems, and do not analyze relativistic quark matter, very similar considerations arise in such an analysis. Indeed, after completion of the work reported here, we learned of closely related work on relativistic systems [18].

In this paper we compute several stability criteria for these states within a simple model field theory. Specifically, we consider a $U(1) \times U(1)$ gauge theory, where each of the gauge fields couples to one of the fermions. These fermions can have different chemical potentials. We work in the mean-field approximation and at zero temperature, but do not restrict ourselves to weak coupling. We compute the electric and magnetic screening mass matrices from the zero-energy, low-momentum limit of the polarization tensor. In quark matter, the Meissner mass has been proven to be a restrictive stability condition at weak coupling: imaginary Meissner masses in the “gapless 2SC” [19] and the “gapless CFL” [20] phases have revealed these phases to be unstable (both phases exhibit breached pairing). We also calculate the number susceptibility matrix, whose positivity provides a second restrictive stability condition. In the normal phase this quantity is identical to the Debye mass but, as we shall discuss in detail, in the super phase these are two different quantities. Finally, we also consider the question of global stability (Clogston limit). We find that there are states which are locally but not globally stable. Such metastable states could be very interesting from an experimental point of view.

In most numerical calculations, the ground state was found by solving the gap equation in the thermodynamic ensemble with fixed particle numbers for both species. In particular, a stable gapless state with one Fermi surface was predicted [5], as well as existence of a gapless state with two Fermi surfaces was deduced from an effective theory [21]. In our analysis, we do not construct the ground state explicitly. Instead we treat chemical potentials and the gap function as parameters, analyzing the whole parameter space systematically for different stability criteria and relating them with the different possible quasiparticle dispersions. We do so for three-dimensional

systems in the main part, Secs. III – V and compare the results with a two-dimensional system in Sec. VII.

When the optimum homogeneous and isotropic state is unstable, the ground state cannot have these properties. Plausible candidates for cold atomic systems include phase separation [13] or a “Larkin-Ovchinnikov-Fulde-Ferrell” (LOFF) state [22], wherein the Cooper pairs carry nonzero total momentum. Whereas a phase-separated state seems unlikely in quark matter because of different color and electric charges of the components, LOFF phases have been discussed both for quark matter [23] and cold atom systems [24, 25].

II. FORMALISM AND DEFINITIONS

A. Order parameter, gauge groups, and partition function

We consider a system of two species of nonrelativistic fermions with Fermi momenta μ_1 and μ_2 and with equal mass m . One can think of these two species as fermions with spin up and spin down. We assume that there is a pointlike attractive interaction between the two species, giving rise to the formation of Cooper pairs. The structure of the pairing order parameter is

$$\Phi^+ = \Delta \sigma_2, \quad (1)$$

where Δ is the gap function and σ_2 is the second Pauli matrix. By choosing σ_2 we only allow for pairing in the singlet channel, i.e., between different fermions. (For the effect of induced intra-species pairing see Ref. [26].) Using the language of spin, this would be the spin-zero channel. The notation Φ^+ will become clear below where we consider fermion fields in Nambu-Gorkov space.

We consider a gauge theory with gauge group $U(1) \times U(1)$. The corresponding gauge fields A_1 and A_2 shall play the role of external fields which are screened in the superconductor. They should not be confused with the interaction that provides the attractive force between the fermions. The gauge group is chosen such that it corresponds to the global group associated with particle number conservation. Therefore, our results regarding stability of the superconductor are valid also for a pure superfluid, i.e., for an analogous system with uncharged fermions. Moreover, the choice of the gauge group enables us to study a possible effect of a mixing of the gauge fields on the stability conditions. The case we consider is the simplest possible to observe this feature. (In quark matter, a more complicated gauge group, $SU(3) \times U(1)$, where $SU(3)$ is the gauge group of the strong interaction and $U(1)$ the electromagnetic gauge group, leads to more complicated mixing patterns of the gauge fields in a color superconductor.)

The two generators of $U(1) \times U(1)$ are

$$T_1 \equiv \begin{pmatrix} 1 & 0 \\ 0 & 0 \end{pmatrix}, \quad T_2 \equiv \begin{pmatrix} 0 & 0 \\ 0 & 1 \end{pmatrix}. \quad (2)$$

This form of the generators implies that the first (second) fermion couples exclusively to the first (second) gauge field A_1 (A_2) with coupling constants g_1 (g_2). Then, the order parameter (1) is invariant under special simultaneous rotations of the subgroups. I.e., with φ_1 and φ_2 being the phases of the two subgroups $U(1)$, the order parameter is invariant, $\sum_{a=1,2} \varphi_a (T_a \sigma_2 + \sigma_2 T_a) = 0$, only if $\varphi_1 = -\varphi_2$. Hence the gauge group is spontaneously broken to a $U(1)$ subgroup,

$$U(1)_{\varphi_1} \times U(1)_{\varphi_2} \rightarrow U(1)_{\varphi_1 - \varphi_2}. \quad (3)$$

Therefore, the two original gauge fields mix with each other, giving rise to two rotated gauge fields in the superconductor. For one of these new gauge fields we expect a vanishing Meissner mass, while the orthogonal new gauge field is expected to attain nonvanishing Meissner mass via the Anderson-Higgs mechanism.

Having defined the structure of the fermion fields and the gauge groups, we may now write down the partition function which, in the subsequent sections, shall serve as a starting point to define the relevant physical quantities. The partition function is

$$\mathcal{Z} = \int \mathcal{D}A e^{S_A} Z_f[A]. \quad (4)$$

The gauge field part e^{S_A} is not relevant for our study and thus does not have to be specified. The fermionic part is

$$\begin{aligned} Z_f[A] = & \int \mathcal{D}\psi^\dagger \mathcal{D}\psi \exp \left(\int_X \left\{ \psi^\dagger \left[i\partial_t \right. \right. \right. \\ & + \frac{1}{2m} (\nabla - i\Gamma_a \mathbf{A}_a)^2 + \Gamma_a A_a^0 + \mu \left. \right] \psi \\ & \left. \left. - g(\psi^\dagger \sigma_2 \psi^*) (\psi^T \sigma_2 \psi) \right\} \right), \end{aligned} \quad (5)$$

where ψ is the two-component fermion field, each component corresponding to one fermion species, and g is the coupling constant of the attractive interaction between different fermion species. The chemical potential is given by the matrix $\mu \equiv \text{diag}(\mu_1, \mu_2)$. The integration over time and space is abbreviated by \int_X , summation over $a = 1, 2$ is implied and $\Gamma_{1/2} \equiv g_{1/2} \tilde{T}_{1/2}$. We have denoted the spatial part of the gauge field by the three-vector \mathbf{A} while the scalar potential is A^0 . Throughout the paper, we work in units of $\hbar = c = k_B = 1$.

B. Propagators, polarization tensor, and screening masses

Next, we introduce the Nambu-Gorkov field, $\Psi = (\psi, \psi^*)$, consisting of a particle and a hole field, and formally integrate out the fermion fields. This yields in the mean-field approximation with $\Delta = 2g\langle\psi^T \sigma_2 \psi\rangle$,

$$\mathcal{Z} = \int \mathcal{D}A \exp \left[S_A + \frac{|\Delta|^2}{4g} - \frac{1}{2} \text{Tr} \ln(\mathcal{S}^{-1} + \mathcal{A}) \right]. \quad (6)$$

The term abbreviated by \mathcal{A} contains the gauge fields and shall be discussed below. First we give the explicit form of the full inverse fermion propagator,

$$\mathcal{S}^{-1} \equiv \begin{pmatrix} [G_0^+]^{-1} & \Phi^- \\ \Phi^+ & [G_0^-]^{-1} \end{pmatrix}, \quad (7)$$

where the Φ^\pm is the order parameter given by Eq. (1), $\Phi^- \equiv (\Phi^+)^\dagger$, and the inverse free fermion propagators are

$$[G_0^\pm]^{-1} = i\partial_t \pm \frac{\nabla^2}{2m} \pm \mu. \quad (8)$$

Note that \mathcal{S}^{-1} is a 4×4 matrix, two degrees of freedom coming from the Nambu-Gorkov structure and explicitly written in Eq. (7), and two degrees of freedom coming from the two fermion species, implicitly present in Eq. (7) through the 2×2 matrices $[G_0^\pm]^{-1}$ and Φ^\pm . In the following, we need the explicit form of the propagator \mathcal{S} in momentum space. Let us denote its Nambu-Gorkov components as follows,

$$\mathcal{S}(K) = \begin{pmatrix} G^+(K) & F^-(K) \\ F^+(K) & G^-(K) \end{pmatrix}, \quad (9)$$

where we use the shorthand notation $K \equiv (k_0, \mathbf{k})$ with $k_0 = -i\omega_n$, ω_n being the fermionic Matsubara frequencies. By inverting Eq. (7) formally, we obtain

$$G^\pm = ([G_0^\pm]^{-1} - \Phi^\mp G_0^\mp \Phi^\pm)^{-1}, \quad (10a)$$

$$F^\pm = -G_0^\mp \Phi^\pm G^\pm. \quad (10b)$$

From Eq. (8) we conclude that, in momentum space, $[G_0^\pm]^{-1} = \text{diag}\{k_0 \mp [k^2/(2m) - \mu_1], k_0 \mp [k^2/(2m) - \mu_2]\}$, where $k \equiv |\mathbf{k}|$. Hence, we find

$$G^\pm = \begin{pmatrix} \frac{k_0 \pm [k^2/(2m) - \mu_2]}{(k_0 \pm \delta\mu)^2 - \epsilon_k^2} & 0 \\ 0 & \frac{k_0 \pm [k^2/(2m) - \mu_1]}{(k_0 \mp \delta\mu)^2 - \epsilon_k^2} \end{pmatrix}, \quad (11a)$$

$$F^\pm = -i\Delta \begin{pmatrix} 0 & -\frac{1}{(k_0 \mp \delta\mu)^2 - \epsilon_k^2} \\ \frac{1}{(k_0 \pm \delta\mu)^2 - \epsilon_k^2} & 0 \end{pmatrix}. \quad (11b)$$

Here and in the following, we use the notation

$$\begin{aligned} \epsilon_k^2 &\equiv \xi_k^2 + \Delta^2, & \xi_k &\equiv \frac{k^2}{2m} - \bar{\mu}, \\ \delta\mu &\equiv \frac{\mu_1 - \mu_2}{2}, & \bar{\mu} &\equiv \frac{\mu_1 + \mu_2}{2}. \end{aligned} \quad (12)$$

Moreover, we have assumed the gap function Δ to be real. In the subsequent sections, we shall make use of these explicit forms of the normal (G^\pm) and anomalous (F^\pm) propagators.

Let us now come back to Eq. (6) in order to define the polarization tensor for the gauge fields. In this equation, we have abbreviated

$$\begin{aligned} \mathcal{A} &\equiv \begin{pmatrix} A^+ & 0 \\ 0 & A^- \end{pmatrix}, \\ A^\pm &\equiv \pm \Gamma_a A_a^0 \mp \frac{\Gamma_a^2}{2m} \mathbf{A}_a^2 \\ &\quad - \frac{i\Gamma_a}{2m} (\nabla \cdot \mathbf{A}_a + \mathbf{A}_a \cdot \nabla). \end{aligned} \quad (13)$$

We perform a derivative expansion, i.e. expand the logarithm in Eq. (6), and collect the terms which are quadratic in the gauge field. Let us denote the sum of these terms by S_2 . After introducing Fourier transforms for the fields $\mathbf{A}_a(X)$, $A_a^0(X)$ and the propagators $S(X, Y)$, and upon assuming translational invariance, $\mathcal{S}(X, Y) = \mathcal{S}(X - Y)$, we can write these terms as

$$S_2 = -\frac{1}{2} \frac{V}{T} \sum_P \left[A_a^0(-P) \Pi_{ab}^{00}(P) A_b^0(P) + A_a^i(-P) \Pi_{ab}^{i0}(P) A_b^0(P) + A_a^0(-P) \Pi_{ab}^{0i}(P) A_b^i(P) + A_a^i(-P) \Pi_{ab}^{ij}(P) A_b^j(P) \right], \quad (14)$$

where we have defined the following components of the polarization tensor Π to one-loop order,

$$\Pi_{ab}^{00}(P) \equiv \frac{1}{2} \frac{T}{V} \sum_K \text{Tr}[S(K) \Gamma_a^- S(K-P) \Gamma_b^-], \quad (15a)$$

$$\begin{aligned} \Pi_{ab}^{i0}(P) &\equiv \frac{1}{2} \frac{T}{V} \sum_K \frac{p_i - 2k_i}{2m} \\ &\times \text{Tr}[S(K) \Gamma_a^+ S(K-P) \Gamma_b^-], \end{aligned} \quad (15b)$$

$$\begin{aligned} \Pi_{ab}^{0i}(P) &\equiv \frac{1}{2} \frac{T}{V} \sum_K \frac{p_i - 2k_i}{2m} \\ &\times \text{Tr}[S(K) \Gamma_a^- S(K-P) \Gamma_b^+], \end{aligned} \quad (15c)$$

$$\begin{aligned} \Pi_{ab}^{ij}(P) &\equiv \frac{1}{2} \frac{T}{V} \sum_K \left\{ \frac{\delta_{ij} \delta_{ab}}{m} \text{Tr}[S(K) \bar{\Gamma}_a^2] \right. \\ &\left. + \frac{(p_i - 2k_i)(p_j - 2k_j)}{4m^2} \text{Tr}[S(K) \Gamma_a^+ S(K-P) \Gamma_b^+] \right\}. \end{aligned} \quad (15d)$$

The traces run over Nambu-Gorkov and two-fermion space, and we have introduced the following matrices in Nambu-Gorkov space,

$$\Gamma_a^\pm \equiv \begin{pmatrix} \Gamma_a & 0 \\ 0 & \pm \Gamma_a \end{pmatrix}, \quad \bar{\Gamma}_a^2 \equiv \begin{pmatrix} \Gamma_a^2 & 0 \\ 0 & -\Gamma_a^2 \end{pmatrix}. \quad (16)$$

In order to compute the electric and magnetic screening masses, we have to compute the 00- and ij -components of the polarization tensor at zero energy, $p_0 = 0$ and for vanishing momentum, $\mathbf{p} \rightarrow 0$. The definitions for the Debye and Meissner masses (squared) are

$$m_{D,ab}^2 \equiv -\lim_{\mathbf{p} \rightarrow 0} \Pi_{ab}^{00}(0, \mathbf{p}), \quad (17a)$$

$$m_{M,ab}^2 \equiv \frac{1}{2} \lim_{\mathbf{p} \rightarrow 0} (\delta_{ij} - \hat{p}_i \hat{p}_j) \Pi_{ab}^{ij}(0, \mathbf{p}), \quad (17b)$$

where $\hat{p}_i \equiv p_i/p$. With $(\delta_{ij} - \hat{p}_i \hat{p}_j) \delta_{ij} = 2$ and $(\delta_{ij} - \hat{p}_i \hat{p}_j)(p_i - 2k_i)(p_j - 2k_j) = 4k^2[1 - (\hat{p} \cdot \hat{k})^2]$ we conclude from Eqs. (15)

$$m_{D,ab}^2 = -\lim_{P \rightarrow 0} \frac{1}{2} \frac{T}{V} \sum_K \text{Tr}[S(K) \Gamma_a^- S(K-P) \Gamma_b^-], \quad (18a)$$

$$m_{M,ab}^2 = \frac{1}{2m} \lim_{P \rightarrow 0} \frac{T}{V} \sum_K \left\{ \delta_{ab} \text{Tr}[S(K) \bar{\Gamma}_a^2] + \frac{k^2}{2m} [1 - (\hat{p} \cdot \hat{k})^2] \text{Tr}[S(K) \Gamma_a^+ S(K-P) \Gamma_b^+] \right\}. \quad (18b)$$

These 2×2 matrices in two-fermion space shall be evaluated in the following sections in order to obtain stability conditions for gapless superconductors.

C. Pressure, gap equation, and number susceptibilities

Besides the screening masses, we shall test the number susceptibility matrix χ on its positive definiteness. In this section, we define χ via the thermodynamic pressure p . One may derive the pressure from the partition function in (4) using the Cornwall-Jackiw-Tomboulis formalism [27]. Employing this formalism results in the effective

potential, being a functional of the fermion and gauge field propagators. The pressure is the negative of the effective potential at its stationary point (i.e., with the propagators determined to extremize the effective potential). The fermionic part of the pressure is

$$p = \frac{1}{2} \frac{T}{V} \text{Tr} \ln \mathcal{S}^{-1} + \frac{1}{2} \frac{T}{V} \text{Tr}[\mathcal{S}_0^{-1} \mathcal{S} - 1] + \Gamma_2[\mathcal{S}], \quad (19)$$

where $\mathcal{S}_0 = \text{diag}(G_0^+, G_0^-)$ is the tree-level fermion propagator in Nambu-Gorkov space with G_0^\pm given in Eq. (8) and $\Gamma_2[\mathcal{S}]$ is the sum of all two-particle irreducible diagrams. The stationarity of the effective potential is ensured by the Schwinger-Dyson equation

$$\mathcal{S}^{-1} = \mathcal{S}_0^{-1} + \Sigma, \quad (20)$$

where

$$\Sigma \equiv 2 \frac{\delta \Gamma_2}{\delta \mathcal{S}} \quad (21)$$

is the fermion self-energy. By making use of the Schwinger-Dyson equation, the pressure can be written as

$$p = \frac{1}{2} \frac{T}{V} \text{Tr} \ln \mathcal{S}^{-1} + \frac{1}{4} \frac{T}{V} \text{Tr} [\mathcal{S}_0^{-1} \mathcal{S} - 1]. \quad (22)$$

From Eqs. (19), (20), (21), and the definition of the number densities

$$n_a = \frac{\partial p}{\partial \mu_a}, \quad (23)$$

we conclude

$$n_a = \frac{1}{2} \frac{T}{V} \text{Tr} \left[\mathcal{S} \frac{\partial \mathcal{S}_0^{-1}}{\partial \mu_a} \right] = \frac{1}{2g_a} \frac{T}{V} \sum_K \text{Tr} [\Gamma_a^- \mathcal{S}(K)]. \quad (24)$$

The number susceptibility χ is defined as the derivative of the number density with respect to the chemical potential (at constant volume and temperature). Hence, making use of

$$\frac{\partial \mathcal{S}}{\partial \mu_b} = -\mathcal{S} \frac{\partial \mathcal{S}^{-1}}{\partial \mu_b} \mathcal{S} = -\mathcal{S} \left(\frac{\Gamma_b^-}{g_b} + \frac{\partial \Sigma}{\partial \mu_b} \right) \mathcal{S}, \quad (25)$$

we obtain

$$\begin{aligned} \chi_{ab} &= \frac{\partial n_a}{\partial \mu_b} = -\frac{1}{2g_a g_b} \frac{T}{V} \sum_K \text{Tr} [\Gamma_a^- \mathcal{S}(K) \Gamma_b^- \mathcal{S}(K)] \\ &\quad - \frac{1}{2g_a} \frac{T}{V} \sum_K \text{Tr} \left[\Gamma_a^- \mathcal{S}(K) \frac{\partial \Sigma(K)}{\partial \mu_b} \mathcal{S}(K) \right]. \end{aligned} \quad (26)$$

The first term on the right-hand side of this equation is given by the one-loop result for the electric screening mass, cf. Eq. (18a). For the second term, we assume that the self-energy Σ depends on μ_b only through the gap Δ , $\frac{\partial \Sigma}{\partial \mu_b} = \frac{\partial \Sigma}{\partial \Delta} \frac{\partial \Delta}{\partial \mu_b}$. Then, with

$$-\mathcal{S} \frac{\partial \Sigma}{\partial \Delta} \mathcal{S} = -\mathcal{S} \frac{\partial \mathcal{S}^{-1}}{\partial \Delta} \mathcal{S} = \frac{\partial \mathcal{S}}{\partial \Delta} \quad (27)$$

we obtain for the susceptibility

$$\chi_{ab} = \frac{m_{D,ab}^2}{g_a g_b} + \frac{\partial n_a}{\partial \Delta} \frac{\partial \Delta}{\partial \mu_b}. \quad (28)$$

In general, the self-energy Σ contains terms of any number of fermion loops. Consequently, the number susceptibility contains terms of arbitrary many fermion loops too, corresponding to the exact Debye mass including

all possible perturbative insertions. Remarkably, the free fermion result for χ , i.e. $\Sigma = 0$, gives the one-loop result for m_D^2 [28]. We shall use Eq. (28) in the following sections to compute the number susceptibility. As this equation shows, it goes beyond the one-loop result for the electric screening mass.

One of the off-diagonal components of Eq. (20) is the self-consistent mean-field gap equation. Using the one-loop approximation for Σ we obtain

$$\Phi^+ = -g \frac{T}{V} \sum_K F^+(K), \quad (29)$$

(The other off-diagonal component of Eq. (20) is simply the hermitian conjugate of this equation.) We shall use this gap equation below.

III. CALCULATION OF SCREENING MASSES AND NUMBER SUSCEPTIBILITIES

A. Screening masses

In this subsection we start from the definitions for the Debye and Meissner masses, Eqs. (18), and derive expressions for these masses that shall be evaluated first in the weak coupling limit, Sec. IV, and then for the general case, Sec. V. In Eqs. (18a) and (18b), we first have to perform the trace over both Nambu-Gorkov and two-particle space. Then, we perform the sum over the fermionic Matsubara frequencies, set $p_0 = 0$, and take the limit $\mathbf{p} \rightarrow 0$. Finally, we take the zero-temperature limit $T \rightarrow 0$. Details of this calculation are deferred to Appendix A. The results are

$$\begin{aligned} m_{D,11}^2 &= \frac{g_1^2}{2} \int \frac{d^3 \mathbf{k}}{(2\pi)^3} \left[\frac{\Delta^2}{2\epsilon_k^3} \Theta(\epsilon_k - \delta\mu) \right. \\ &\quad \left. + \frac{(\epsilon_k + \xi_k)^2}{2\epsilon_k^2} \delta(\epsilon_k - \delta\mu) \right], \end{aligned} \quad (30a)$$

$$\begin{aligned} m_{D,22}^2 &= \frac{g_2^2}{2} \int \frac{d^3 \mathbf{k}}{(2\pi)^3} \left[\frac{\Delta^2}{2\epsilon_k^3} \Theta(\epsilon_k - \delta\mu) \right. \\ &\quad \left. + \frac{(\epsilon_k - \xi_k)^2}{2\epsilon_k^2} \delta(\epsilon_k - \delta\mu) \right], \end{aligned} \quad (30b)$$

$$\begin{aligned} m_{D,12}^2 &= m_{D,21}^2 = \frac{g_1 g_2}{2} \\ &\times \int \frac{d^3 \mathbf{k}}{(2\pi)^3} \left[\frac{\Delta^2}{2\epsilon_k^3} \Theta(\epsilon_k - \delta\mu) - \frac{\Delta^2}{2\epsilon_k^2} \delta(\epsilon_k - \delta\mu) \right]. \end{aligned} \quad (30c)$$

and

$$m_{M,11}^2 = \frac{g_1^2}{2m} \int \frac{d^3\mathbf{k}}{(2\pi)^3} \left[\frac{\epsilon_k - \xi_k}{\epsilon_k} + \frac{\epsilon_k + \xi_k}{\epsilon_k} \Theta(\delta\mu - \epsilon_k) \right] - \frac{g_1^2}{2m} \int \frac{d^3\mathbf{k}}{(2\pi)^3} \frac{k^2 \sin^2 \theta_{\mathbf{k}}}{2m} \left[\frac{\Delta^2}{2\epsilon_k^3} \Theta(\epsilon_k - \delta\mu) + \frac{(\epsilon_k + \xi_k)^2}{2\epsilon_k^2} \delta(\epsilon_k - \delta\mu) \right], \quad (31a)$$

$$m_{M,22}^2 = \frac{g_2^2}{2m} \int \frac{d^3\mathbf{k}}{(2\pi)^3} \frac{\epsilon_k - \xi_k}{\epsilon_k} \Theta(\epsilon_k - \delta\mu) - \frac{g_2^2}{2m} \int \frac{d^3\mathbf{k}}{(2\pi)^3} \frac{k^2 \sin^2 \theta_{\mathbf{k}}}{2m} \left[\frac{\Delta^2}{2\epsilon_k^3} \Theta(\epsilon_k - \delta\mu) + \frac{(\epsilon_k - \xi_k)^2}{2\epsilon_k^2} \delta(\epsilon_k - \delta\mu) \right], \quad (31b)$$

$$m_{M,12}^2 = m_{M,21}^2 = \frac{g_1 g_2}{2m} \int \frac{d^3\mathbf{k}}{(2\pi)^3} \frac{k^2 \sin^2 \theta_{\mathbf{k}}}{2m} \left[\frac{\Delta^2}{2\epsilon_k^3} \Theta(\epsilon_k - \delta\mu) - \frac{\Delta^2}{2\epsilon_k^2} \delta(\epsilon_k - \delta\mu) \right], \quad (31c)$$

where the notation from Eq. (12) has been used. Without loss of generality, we have assumed $\mu_1 \geq \mu_2$, hence $\delta\mu \geq 0$. Furthermore, we subtracted the vacuum contribution in the first integrals on the right-hand sides of Eqs. (31a) and (31b).

We introduce the dimensionless variables

$$\rho \equiv \frac{\bar{\mu}}{\Delta}, \quad \eta \equiv \frac{\delta\mu}{\Delta}. \quad (32)$$

In the following we shall discuss all our results in terms of these variables. It might seem unconventional to normalize both $\bar{\mu}$ and $\delta\mu$ with respect to the gap Δ . However, for our purpose, this is the most convenient choice. As shall be clear from the following, this choice enables us to present both different Fermi surface topologies as well as stability criteria in a single plot, i.e., without having to choose specific values for parameters such as the fermion mass and the energy gap.

While $\eta \geq 0$, ρ can be both positive or negative, because $\bar{\mu}$ assumes negative values in the BEC regime. Moreover, we abbreviate

$$\rho_{\pm} \equiv \rho \pm \sqrt{\eta^2 - 1}, \quad (33)$$

and define the integrals

$$I_{\rho}(a, b) \equiv \int_a^b dx \frac{x^2}{[(x^2 - \rho)^2 + 1]^{3/2}}, \quad (34a)$$

$$\tilde{I}_{\rho}(a, b) \equiv \int_a^b dx \frac{x^4}{[(x^2 - \rho)^2 + 1]^{3/2}}. \quad (34b)$$

The angular integration in Eqs. (30) and (31) is trivial. The integration over the modulus of the fermion momentum k can be done analytically for all terms that contain the δ -function. To this end, we use the general formula

$$\int_0^{\infty} dk k^n \delta(\epsilon_k - \delta\mu) f(k) = m (2m\Delta)^{(n-1)/2} \times \Theta(\eta - 1) \frac{\eta}{\sqrt{\eta^2 - 1}} \left[\Theta(\rho_+) \rho_+^{(n-1)/2} f(\sqrt{2m\Delta} \rho_+) + \Theta(\rho_-) \rho_-^{(n-1)/2} f(\sqrt{2m\Delta} \rho_-) \right], \quad (35)$$

where f is an arbitrary function, e.g., $f(k) = \Delta^2/(2\epsilon_k^2)$, and n assumes the values $n = 2, 4$. The integrals in Eqs. (30) and (31) with a Θ -function lead to elliptic integrals. In general,

$$\int_0^{\infty} dk k^n \Theta(\epsilon_k - \delta\mu) f(k) = (2m\Delta)^{(n+1)/2} \times \{ F_n(0, \infty) - \Theta(\eta - 1) [\Theta(\rho_+) F_n(0, \sqrt{\rho_+}) - \Theta(\rho_-) F_n(0, \sqrt{\rho_-})] \}, \quad (36)$$

where again f is an arbitrary function, e.g., $f(k) = \Delta^2/(2\epsilon_k^3)$, and

$$F_n(a, b) \equiv \int_a^b dx x^n f(\sqrt{2m\Delta} x). \quad (37)$$

The results (35) and (36) show that different terms are switched on or off by the Θ -functions, depending on whether η is larger or smaller than 1 and whether ρ_+ and ρ_- are positive or negative. These conditions can be directly translated into the topology of the effective Fermi surfaces, as we demonstrate now. From the denominators in the propagators in Eq. (11) we conclude that there are two quasiparticle excitation energies,

$$\epsilon_k^{\pm} \equiv \sqrt{\left(\frac{k^2}{2m} - \bar{\mu} \right)^2 + \Delta^2 \pm \delta\mu}. \quad (38)$$

It is obvious that, for any values of $\Delta > 0$, $\bar{\mu}$ and $\delta\mu > 0$, the first excitation branch ϵ_k^+ has no zero. This is the usual situation in a conventional superconductor: Quasiparticles at the Fermi surface have a finite excitation energy, given by Δ (and here enhanced by $\delta\mu$). The second quasiparticle dispersion ϵ_k^- , however, is more interesting. Depending on the values of Δ , $\bar{\mu}$, and $\delta\mu$ it can have either no, one, or two zeroes. A zero of ϵ_k^- leads to an effective Fermi surface in the superconducting state. Since we consider isotropic systems, this surface is a sphere. We illustrate the possible dispersion relations in Fig. 1. In Fig. 2, we show the corresponding quasiparticle occupation numbers. [Their formal expression is encountered

in the calculation of the number susceptibilities, see integrands on the right-hand sides of Eqs. (46).]

We can classify the different Fermi surface topologies with the help of the dimensionless parameters:

- *No effective Fermi surface (region F_0 in Fig. 3)*

$$\eta < 1 \quad \text{or} \quad \eta > 1, \quad \rho_+, \rho_- < 0. \quad (39)$$

The first case, $\eta < 1$, translates into $\delta\mu < \Delta$ and includes the usual BCS superconductivity. In the second case, $\eta > 1$, ϵ_k^- has no zeroes provided the average chemical potential is sufficiently small, $\bar{\mu} < -\sqrt{\delta\mu^2 - \Delta^2}$.

- *One effective Fermi surface (region F_1 in Fig. 3)*

$$\eta > 1, \quad \rho_+ > 0, \quad \rho_- < 0. \quad (40)$$

This case requires a sufficiently large mismatch of chemical potentials, $\delta\mu > \Delta$, and sets an upper and lower limit for the average chemical potential, $-\sqrt{\delta\mu^2 - \Delta^2} < \bar{\mu} < \sqrt{\delta\mu^2 - \Delta^2}$. The latter condition cannot be fulfilled in the weak coupling regime. The case of one effective Fermi surface is characterized by unpaired fermions of the first species, occupying the entire effective Fermi sphere in momentum space [5, 21].

- *Two effective Fermi surfaces (region F_2 in Fig. 3)*

$$\eta > 1, \quad \rho_+, \rho_- > 0. \quad (41)$$

This case is the breached pairing phase [6]. Here, the average chemical potential has a lower bound, $\sqrt{\delta\mu^2 - \Delta^2} < \bar{\mu}$. Unpaired fermions of the first species occupy the states between the two Fermi spheres in momentum space.

Having classified the different topologies with respect to the dimensionless quantities, we may now present the general results for the Debye and Meissner masses. In order to avoid a complicated notation we may omit all Θ -functions. The rule they impose on the following expressions is simple:

- For the case of no effective Fermi surface, set $\rho_+ = \rho_- = 0$.
- For the case of one effective Fermi surface, set $\rho_- = 0$ (and keep ρ_+).
- For the case of two effective Fermi surfaces, keep all terms.

These rules are obvious in view of the explicit expressions (35) and (36) and the above classifications. In other words, the following expressions are, strictly speaking, only valid in region F_2 , but the results for regions F_0 and F_1 can be obtained immediately applying the above rules.

From now on, for the sake of simplicity, we set the coupling constants $g_1 = g_2 = 1$. The result for the Debye mass is then straightforwardly derived as

$$\frac{m_{D,11/22}^2}{M_D^2} = I + \frac{(\eta \pm \sqrt{\eta^2 - 1})^2}{2\eta\sqrt{\eta^2 - 1}} \sqrt{\rho_+} + \frac{(\eta \mp \sqrt{\eta^2 - 1})^2}{2\eta\sqrt{\eta^2 - 1}} \sqrt{\rho_-}, \quad (42a)$$

$$\frac{m_{D,12}^2}{M_D^2} = \frac{m_{D,21}^2}{M_D^2} = I - \frac{\sqrt{\rho_+} + \sqrt{\rho_-}}{2\eta\sqrt{\eta^2 - 1}}. \quad (42b)$$

The result for the Meissner mass becomes amazingly simple after rewriting some of the integrals. We show the details of this derivation in Appendix B. The result is

$$\frac{m_{M,ab}^2}{M_M^2} = \tilde{I} - \frac{\rho_+^{3/2} + \rho_-^{3/2}}{2\eta\sqrt{\eta^2 - 1}}. \quad (43)$$

We abbreviated

$$I \equiv I_\rho(0, \infty) - I_\rho(\sqrt{\rho_-}, \sqrt{\rho_+}), \quad (44a)$$

$$\tilde{I} \equiv \tilde{I}_\rho(0, \infty) - \tilde{I}_\rho(\sqrt{\rho_-}, \sqrt{\rho_+}), \quad (44b)$$

and normalized the screening masses with the quantities

$$M_D^2 \equiv \frac{m^{3/2}\Delta^{1/2}}{2\sqrt{2}\pi^2}, \quad M_M^2 \equiv \frac{m^{1/2}\Delta^{3/2}}{3\sqrt{2}\pi^2}. \quad (45)$$

Since $M_D^2, M_M^2 > 0$, and since we are interested in the positive definiteness of the screening mass matrices, we can continue our analysis with the normalized quantities.

B. Number susceptibilities

In this subsection we start from the definition of the number susceptibilities (28) and compute the matrix χ_{ab} in order to evaluate it in Secs. IV and V. From Eqs. (42) we already know the first term on the right-hand side of Eq. (28). The second term is computed as follows. For the derivative $\partial n_a / (\partial \mu_b)$ we make use of the fact that the density n_a has basically already been computed in the calculation of the Meissner mass, cf. Eqs. (18b) and (24). Therefore, from Eqs. (31a) and (31b) we read off

$$n_1 = \frac{1}{2} \int \frac{d^3\mathbf{k}}{(2\pi)^3} \left[\frac{\epsilon_k - \xi_k}{\epsilon_k} + \frac{\epsilon_k + \xi_k}{\epsilon_k} \Theta(\delta\mu - \epsilon_k) \right] \quad (46a)$$

$$n_2 = \frac{1}{2} \int \frac{d^3\mathbf{k}}{(2\pi)^3} \frac{\epsilon_k - \xi_k}{\epsilon_k} \Theta(\epsilon_k - \delta\mu). \quad (46b)$$

Now we straightforwardly take the derivative of the right-hand side of these equations with respect to Δ . The

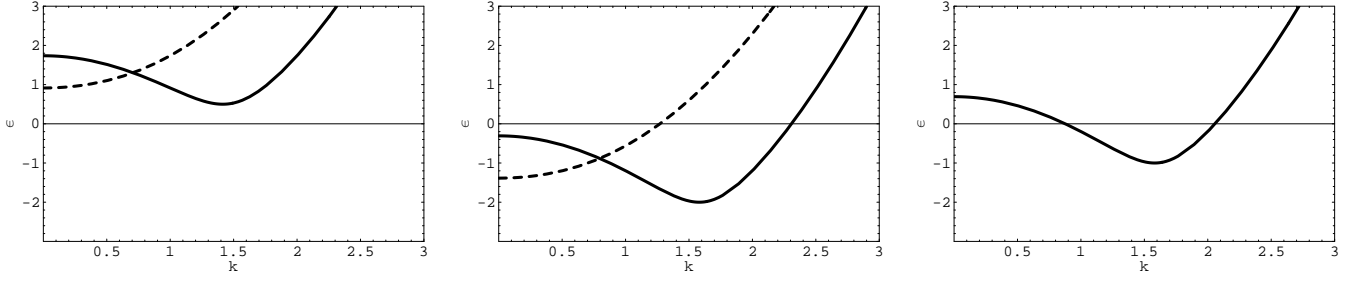


FIG. 1: Schematic plot of possible quasiparticle dispersion relations ϵ_k^- (in arbitrary units). From left to right, the dispersions correspond to states with zero, one, and two effective Fermi surfaces (zeroes of ϵ_k^-). For zero and one effective Fermi surface, two qualitatively different dispersions are possible, distinguished by the location of their minimum k_0 . In each case, the solid (dashed) line corresponds to $k_0 \neq 0$ ($k_0 = 0$) and a positive (negative) $\bar{\mu}$. From left to right, the parameter ranges are given by Eqs. (39), (40), and (41), respectively.

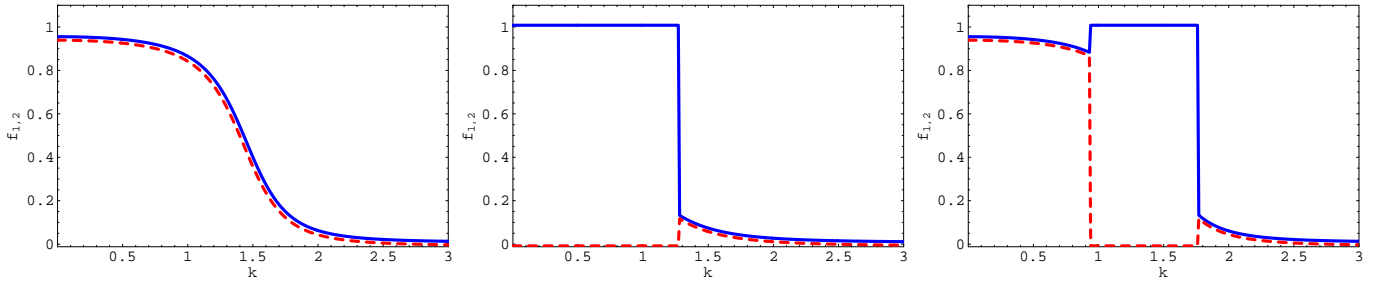


FIG. 2: (Color online) Schematic plot of possible quasiparticle occupation numbers (in arbitrary units). With $\mu_1 > \mu_2$, f_1 (f_2) corresponds to the solid, blue online, (dashed, red online) curves. From left to right, analogous to Fig. 1, the occupation numbers correspond to states with zero, one, and two effective Fermi surfaces, respectively. (Where both occupation numbers are identical, e.g., for all k in the left panel, we have shifted their value slightly for illustrative purposes.)

result, again normalized with the help of M_D^2 and written in dimensionless quantities, is

$$\frac{1}{M_D^2} \frac{\partial n_{1/2}}{\partial \Delta} = 2(\tilde{I} - \rho I) \mp 2 \left(\frac{\eta \pm \sqrt{\eta^2 - 1}}{2\eta\sqrt{\eta^2 - 1}} \sqrt{\rho_+} + \frac{\eta \mp \sqrt{\eta^2 - 1}}{2\eta\sqrt{\eta^2 - 1}} \sqrt{\rho_-} \right). \quad (47)$$

For the derivative $\partial \Delta / (\partial \mu_b)$ we make use of the gap equation (29). In order to extract the equation for Δ from this matrix equation, we multiply both sides with σ_2 and take the trace. Then, after performing the Matsubara sum and taking the zero-temperature limit, the gap equation reads

$$-\frac{1}{g} = \int \frac{d^3 \mathbf{k}}{(2\pi)^3} \frac{1}{2\epsilon_k} \Theta(\epsilon_k - \delta\mu). \quad (48)$$

We may rewrite the gap equation in terms of the s -wave scattering length a which is given by

$$\frac{m}{4\pi a} = \frac{1}{g} + \frac{1}{V} \sum_{\mathbf{k}} \frac{m}{k^2}. \quad (49)$$

Then, the gap equation becomes

$$-\frac{m}{4\pi a} = \int \frac{d^3 \mathbf{k}}{(2\pi)^3} \left[\frac{1}{2\epsilon_k} \Theta(\epsilon_k - \delta\mu) - \frac{m}{k^2} \right]. \quad (50)$$

Although not necessary in the current calculation, this rewriting is crucial in order to solve the gap equation (see Sec. V) since it provides a natural regularization for the otherwise divergent integral (unlike the weak coupling case, where a natural cut-off is provided by the Debye frequency). We may now use Eq. (50), or, in this case, equivalently, Eq. (48) and take the derivative with respect to μ_b on both sides of the equation to obtain

$$\frac{\partial \Delta}{\partial \mu_{1/2}} = \frac{1}{2} \left(I - \frac{\sqrt{\rho_+} + \sqrt{\rho_-}}{2\eta\sqrt{\eta^2 - 1}} \right)^{-1} \left[\tilde{I} - \rho I \mp \left(\frac{\eta \pm \sqrt{\eta^2 - 1}}{2\eta\sqrt{\eta^2 - 1}} \sqrt{\rho_+} + \frac{\eta \mp \sqrt{\eta^2 - 1}}{2\eta\sqrt{\eta^2 - 1}} \sqrt{\rho_-} \right) \right]. \quad (51)$$

It is convenient to consider a susceptibility matrix $\tilde{\chi}$ defined in terms of $n \equiv n_1 + n_2$, $\delta n \equiv n_1 - n_2$, and $\bar{\mu}$, $\delta\mu$ rather than χ which is defined in terms of n_1 , n_2 , μ_1 , μ_2 .

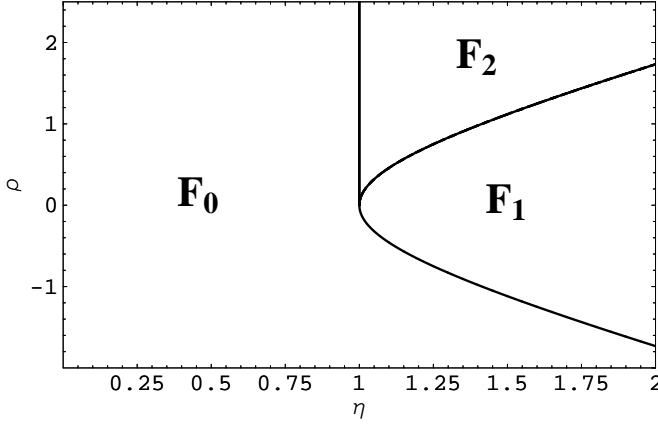


FIG. 3: Different topologies of the effective Fermi surfaces in the $\rho\eta$ -plane, $\rho = \bar{\mu}/\Delta$, $\eta = \delta\mu/\Delta$. Phases in the regions F_0 , F_1 , and F_2 have zero, one, or two effective Fermi surfaces, respectively. Region F_1 is bounded by the lines $\rho_+ = 0$ and $\rho_- = 0$.

The relation between $\tilde{\chi}$ and χ is

$$\tilde{\chi} = Q \chi Q, \quad Q \equiv \begin{pmatrix} 1 & 1 \\ 1 & -1 \end{pmatrix}, \quad (52)$$

where the entries of χ are given in Eq. (28). Inserting the results (42), (47), and (51) into Eq. (28) and using the transformation (52) we obtain

$$\frac{\tilde{\chi}}{M_D^2} = \frac{4}{R} \begin{pmatrix} \omega_{11} & \omega_{12} \\ \omega_{21} & \omega_{22} \end{pmatrix}, \quad (53)$$

where

$$R \equiv I - \frac{\sqrt{\rho_+} + \sqrt{\rho_-}}{2\eta\sqrt{\eta^2 - 1}}, \quad (54)$$

and

$$\begin{aligned} \omega_{11} \equiv & I^2 + (\tilde{I} - \rho I)^2 + I \frac{\eta^2 - 2}{2\eta\sqrt{\eta^2 - 1}}(\sqrt{\rho_+} + \sqrt{\rho_-}) \\ & - (\tilde{I} - \rho I) \frac{\sqrt{\rho_+} - \sqrt{\rho_-}}{\eta} - \frac{\sqrt{\rho_+}\sqrt{\rho_-}}{\eta^2}, \end{aligned} \quad (55a)$$

$$\omega_{22} \equiv I \frac{\eta}{2\sqrt{\eta^2 - 1}}(\sqrt{\rho_+} + \sqrt{\rho_-}), \quad (55b)$$

$$\begin{aligned} \omega_{12} = \omega_{21} \equiv & I \frac{\sqrt{\rho_+} - \sqrt{\rho_-}}{2} \\ & - (\tilde{I} - \rho I) \frac{\sqrt{\rho_+} + \sqrt{\rho_-}}{2\sqrt{\eta^2 - 1}}. \end{aligned} \quad (55c)$$

This result shall be used in the subsequent sections.

IV. WEAK COUPLING LIMIT

Before evaluating the results of the previous section in full generality, let us first discuss the weak coupling, or BCS, limit. This limit is characterized by a fixed average chemical potential $\bar{\mu}$ which is much larger than both the mismatch $\delta\mu$ and the gap Δ . From this property we conclude that the scenario with a single effective Fermi surface is not possible. This scenario is only possible in the strong coupling regime. However, besides the ordinary superconducting phase without gapless excitation, there is the possibility of a gapless phase with two effective Fermi surfaces. This situation occurs for sufficiently large mismatches $\delta\mu > \Delta$, or $\eta > 1$.

In terms of the above introduced dimensionless parameters, the BCS limit yields the following simple approximations for the integrals defined in Eq. (34),

$$I_\rho(0, \infty) \simeq \sqrt{\rho}, \quad (56a)$$

$$I_\rho(\sqrt{\rho_-}, \sqrt{\rho_+}) \simeq \sqrt{\rho} \frac{\sqrt{\eta^2 - 1}}{\eta}, \quad (56b)$$

$$\tilde{I}_\rho(0, \infty) \simeq \rho^{3/2}, \quad (56c)$$

$$\tilde{I}_\rho(\sqrt{\rho_-}, \sqrt{\rho_+}) \simeq \rho^{3/2} \frac{\sqrt{\eta^2 - 1}}{\eta}. \quad (56d)$$

In all other terms we may approximate

$$\rho_- \simeq \rho_+ \simeq \rho. \quad (57)$$

Using these approximations, we can immediately compute explicitly the screening mass matrices as well as the number susceptibility matrix from Eqs. (42), (43), and (53). Remember that in all these equations we omitted the Θ -functions. In order to compute the BCS limit results, we reinstall the factor $\Theta(\eta - 1)$ in front of all terms that contain ρ_- or ρ_+ . Because of $\bar{\mu} \gg \delta\mu, \Delta$ we have $\Theta(\rho_+) = \Theta(\rho_-) = 1$. Then, we obtain for the Debye mass matrix

$$\frac{m_{D,11/22}^2}{M_D^2} \simeq \sqrt{\rho} \left(1 + \frac{\Theta(\eta - 1)\eta}{\sqrt{\eta^2 - 1}} \right), \quad (58a)$$

$$\frac{m_{D,12/21}^2}{M_D^2} \simeq \sqrt{\rho} \left(1 - \frac{\Theta(\eta - 1)\eta}{\sqrt{\eta^2 - 1}} \right), \quad (58b)$$

which leads to the eigenvalues

$$\frac{m_{D,1}^2}{M_D^2} \simeq 2\sqrt{\rho}, \quad \frac{m_{D,2}^2}{M_D^2} \simeq 2\sqrt{\rho} \frac{\Theta(\eta - 1)\eta}{\sqrt{\eta^2 - 1}}, \quad (59)$$

which both are positive for all values of the mismatch η .

For the Meissner masses, we obtain

$$\frac{m_{M,ab}^2}{M_M^2} \simeq \rho^{3/2} \left(1 - \frac{\Theta(\eta - 1)\eta}{\sqrt{\eta^2 - 1}} \right), \quad (60)$$

leading to the eigenvalues

$$\frac{m_{M,1}^2}{M_M^2} \simeq 2\rho^{3/2} \left(1 - \frac{\Theta(\eta - 1)\eta}{\sqrt{\eta^2 - 1}} \right), \quad \frac{m_{M,2}^2}{M_M^2} \simeq 0. \quad (61)$$

Hence, in the weak coupling limit, the magnetic screening mass matrix is positive definite if and only if the spectrum is fully gapped, $\eta < 1$ [30]. This result is similar to the behavior of the gluon Meissner masses in two- and three-flavor color-superconducting quark matter [19, 20]. (However, in a two-flavor color superconductor the situation is more complicated, because some of the gluon Meissner masses become imaginary even in the fully gapped region. The nature of this different kind of instability has been analyzed in Ref. [31].) The result has also been discussed in the context of superfluids, where the role of the Meissner mass squared is played by the density of superfluid fermions [8, 32, 33].

Finally, for the number susceptibility matrix in the weak coupling limit we find

$$\sqrt{\rho} R \simeq \omega_{11} \simeq \rho \left[1 - \frac{\Theta(\eta - 1) \eta}{\sqrt{\eta^2 - 1}} \right], \quad (62a)$$

$$\omega_{22} \simeq -\rho \Theta(\eta - 1) \left(1 - \frac{\eta}{\sqrt{\eta^2 - 1}} \right), \quad (62b)$$

$$\omega_{12} = \omega_{21} \simeq 0, \quad (62c)$$

and hence

$$\frac{\tilde{\chi}}{M_D^2} \simeq 4\sqrt{\rho} \begin{pmatrix} 1 & 0 \\ 0 & -\Theta(\eta - 1) \end{pmatrix}. \quad (63)$$

This matrix shows that the gapped state is stable, while the gapless state is unstable, which is the same conclusion that can be drawn from the Meissner mass matrix. The negative value in $\tilde{\chi}$ corresponds to a negative derivative of δn with respect to $\delta\mu$, meaning that, in a potential gapless state, an increase in the mismatch of chemical potentials would lead to a decrease in the mismatch of number densities. It agrees with physical intuition that this cannot be possible.

V. STABILITY CONDITIONS

In this section, we use the results from Sec. III to analyze the stability of a superconducting state with a given mismatch in chemical potentials and a given average chemical potential. This will result in a two-dimensional phase diagram with stable and unstable regions. The analysis goes beyond the BCS limit of the previous section by allowing for arbitrary values of the mismatch and chemical potentials. In particular, we generalize the results to the BEC regime (however, of course, relying still on the mean-field results of the previous sections). Moreover, we solve the gap equation, which we present, for given coupling strengths, as lines in the phase diagram.

A. Stability with respect to the screening masses

Both the Debye and Meissner mass matrix are required to be positive definite, i.e., both eigenvalues of each of

these 2×2 matrices have to be positive. The eigenvalues of the 2×2 screening mass matrices m_I^2 ($I = D, M$) are given by

$$m_{I,1/2}^2 = \frac{\text{Tr } m_I^2}{2} \pm \sqrt{\left(\frac{\text{Tr } m_I^2}{2} \right)^2 - \text{Det } m_I^2}. \quad (64)$$

Since the matrices we consider are real and symmetric, both eigenvalues are real, i.e., the argument of the square root in Eq. (64) is positive. Hence, $m_{I,1}^2 > m_{I,2}^2$, and both eigenvalues are positive if and only if both $\text{Tr } m_I^2$ and $\text{Det } m_I^2$ are positive. We use Eqs. (42) to compute trace and determinant for the Debye mass matrix. We obtain

$$\frac{\text{Tr } m_D^2}{M_D^2} = 2I + \frac{2\eta^2 - 1}{\eta\sqrt{\eta^2 - 1}}(\sqrt{\rho_+} + \sqrt{\rho_-}), \quad (65a)$$

$$\frac{\text{Det } m_D^2}{M_D^4} = I \frac{2\eta}{\sqrt{\eta^2 - 1}}(\sqrt{\rho_+} + \sqrt{\rho_-}) + 4\sqrt{\rho_+}\sqrt{\rho_-}. \quad (65b)$$

These expressions can be translated immediately into all three different topologies of the effective Fermi surfaces, see text above Eq. (42). In particular, the second term on the right-hand side of Eq. (65a) is “switched on” only for $\eta > 1$. Thus this term is positive. Also the integral I is positive, see definitions (34a) and (44a). Consequently, both trace and determinant are positive for any pair of parameters ρ , η and hence the Debye mass matrix is positive definite.

The eigenvalues of the Meissner mass matrix are easily computed from Eq. (43). This equation shows that all four entries of the matrix are identical. Therefore, one of the eigenvalues is zero, while the other one is twice the right-hand side of Eq. (43). This is in accordance with the general argument presented in Sec. II A. It reflects the unbroken group $U(1)_{\varphi_1 - \varphi_2}$. In other words, there is no Meissner effect for one special admixture of the original gauge fields. The nonvanishing second eigenvalue corresponds to the orthogonal admixture. Note that the mixing between the magnetic part of the gauge fields does not depend on ρ and η (it only depends on the coupling constants g_1 , g_2 , which we have omitted here). This is in contrast to the mixing in the electric sector. From the above results for the Debye mass, Eqs. (42), we see that the mixing depends on ρ and η . Only in a fully gapped superconductor, where Eqs. (42) reduce to $m_{D,ab}^2/M_D^2 = I_\rho(0, \infty)$, the mixing is identical to the magnetic sector. Also in a two-flavor color superconductor the mixing in the electric sector depends, in contrast to the magnetic sector, on the mismatch, shown for the weak coupling limit in Ref. [19]. However, in this case, different mixing angles of electric and magnetic sectors are observed even in the fully gapped phase [34].

The stability with respect to the Meissner mass is analyzed by checking the sign of the nonzero eigenvalue, i.e., the sign of the right-hand side of Eq. (43). It is obvious

that this eigenvalue is positive for a fully gapped excitation spectrum, because \tilde{I} is positive, see definitions (34b) and (44b). It can be checked numerically that the eigenvalue is also positive in the case of one Fermi surface, i.e., setting $\rho_- = 0$ in Eq. (43). The most interesting case is the breached phase. In this case there is a region in the parameter space where the eigenvalue is negative, indicating a magnetic instability. This region is separated from the stable region by a line in the $\rho\eta$ -plane, given by the (numerical) solution to the equation

$$\tilde{I}_\rho(0, \infty) - \tilde{I}_\rho(\sqrt{\rho_-}, \sqrt{\rho_+}) - \frac{\rho_+^{3/2} + \rho_-^{3/2}}{2\eta\sqrt{\eta^2 - 1}} = 0. \quad (66)$$

The solution is given by the dashed-dotted (blue online) curve in Fig. 4. It renders all phases between the black vertical and the dashed-dotted line unstable with respect to the Meissner mass. However, this stability criterion leaves an apparently stable breached pair region in the phase diagram (shaded in light gray).

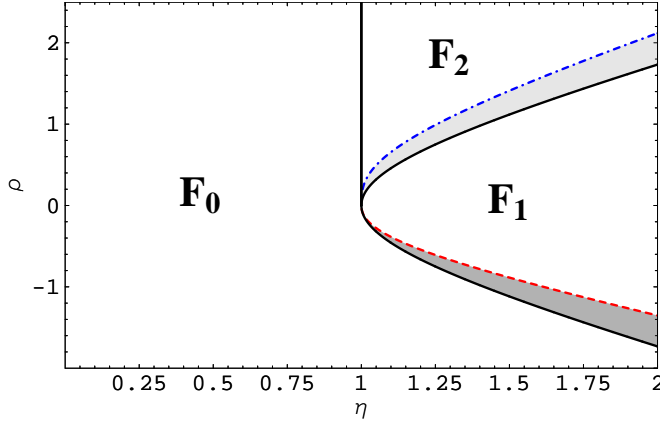


FIG. 4: (Color online) Stability conditions in the $\rho\eta$ -plane. Solid lines and regions F_0 , F_1 , F_2 are taken from Fig. 3. The region between the solid vertical line and the dashed-dotted (blue online) curve is unstable with respect to a negative Meissner mass squared. The region shaded in light gray contains breached pair states that are stable with respect to the Meissner mass. The region between the solid vertical line and the dashed (red online) line is unstable with respect to a negative number susceptibility. The region shaded in dark gray contains gapless states with one Fermi sphere that are stable with respect to the number susceptibility. Remember $\rho = \bar{\mu}/\Delta$, $\eta = \delta\mu/\Delta$.

B. Stability with respect to the number susceptibility

In this subsection we test the susceptibility matrix (53) on its positive definiteness. From the transformation (52) it is obvious that $\tilde{\chi}$ is positive definite if and only if χ is positive definite (note that $Q^2 = 2$). So we may restrict our analysis to $\tilde{\chi}$. Again, the simplest case is the

one without zero in the dispersion relations. In this case, there is only one nonzero entry in the susceptibility matrix. This entry is positive for all ρ (and independent of η),

$$\frac{\tilde{\chi}_{11}}{M_D^2} = 4 \frac{I_\rho^2(0, \infty) + [\tilde{I}_\rho(0, \infty) - \rho I_\rho(0, \infty)]^2}{I_\rho(0, \infty)}, \quad (67a)$$

$$\tilde{\chi}_{12} = \tilde{\chi}_{21} = \tilde{\chi}_{22} = 0. \quad (67b)$$

The most convenient way to determine the sign of the eigenvalues of $\tilde{\chi}$ in the other two cases is to write them as

$$\frac{\tilde{\chi}_{1/2}}{M_D^2} = \frac{4}{R} \left[\frac{\text{Tr } \omega}{2} \pm \sqrt{\left(\frac{\text{Tr } \omega}{2}\right)^2 - \text{Det } \omega} \right]. \quad (68)$$

where the entries of the 2×2 matrix ω are given by Eqs. (55), and R is defined in Eq. (54). For two effective Fermi surfaces, it is a simple numerical task to determine the signs of $\text{Det } \omega$ and R . Both quantities turn out to be negative throughout the parameter region of interest. Consequently, independent of the sign of $\text{Tr } \omega$, at least one eigenvalue is negative, rendering the complete parameter region of two effective Fermi surfaces unstable.

For one effective Fermi surface, one can show numerically that $\text{Tr } \omega$ is positive throughout the parameter region. The determinant can be written as

$$\text{Det } \omega = R \frac{\eta\sqrt{\rho_+}}{2\sqrt{\eta^2 - 1}} \left\{ I_\rho^2(\sqrt{\rho_+}, \infty) + [\tilde{I}_\rho(\sqrt{\rho_+}, \infty) - \rho I_\rho(\sqrt{\rho_+}, \infty)]^2 \right\}. \quad (69)$$

This expression is very useful because it enables us to find a simple condition for the positivity of $\tilde{\chi}$ without computing the eigenvalues explicitly. From Eq. (69) it is clear that $\text{Det } \omega$ is positive if and only if R is positive. Therefore, the positivity of $\tilde{\chi}$ reduces to the positivity of R : If $R < 0$, one of the eigenvalues of $\tilde{\chi}$ is negative, while for $R > 0$ both eigenvalues are positive. Hence, using the definition for R , Eq. (54), stable and unstable regions in the $\rho\eta$ -plane are separated by the solution of the equation

$$I_\rho(\sqrt{\rho_+}, \infty) - \frac{\sqrt{\rho_+}}{2\eta\sqrt{\eta^2 - 1}} = 0. \quad (70)$$

Interestingly, the structure of this equation is very similar to that of Eq. (66). The dashed (red online) line in Fig. 4 represents the solutions to Eq. (70). Consequently, the region between the solid vertical line and the dashed curve is unstable. This result shows that the number susceptibility alone would have been sufficient to determine stable and unstable regions of the phase diagram in our approach. It is interesting to see that neither of the stability conditions exactly coincides with the topology of the dispersion relation. In other words, the lines that separate stable from unstable regions are close to,

but not on top of the lines that separate regions of different topology. The conclusion in terms of topology is that the entire region without an effective Fermi surface is stable, not a single point in the region with two effective Fermi surfaces (“breach”) is stable, and a subset of the region with one effective Fermi surface is stable. This subset only contains phases with negative average chemical potential. We recall that, within our assumption of a homogeneous system, we are not able to make predictions about the true ground states in the unstable region. In the context of cold atoms, it can be expected that a negative Meissner mass squared leads to a LOFF state [24, 25, 35], while a negative number susceptibility leads to phase separation [13, 24].

At the end of this section, we note that, in the considered model, the positivity of the number susceptibility corresponds to a local maximum of the pressure. This can be seen explicitly as follows. We start from Eq. (22), insert the propagators, Eqs. (9) and (11), take the trace, perform the Matsubara sum, and take the zero-temperature limit. This yields

$$p = \int \frac{d^3\mathbf{k}}{(2\pi)^3} \left[\left(\epsilon_k - \frac{\Delta^2}{2\epsilon_k} \right) \Theta(\epsilon_k - \delta\mu) + \delta\mu \Theta(\delta\mu - \epsilon_k) \right]. \quad (71)$$

We find that the second derivative of the pressure with respect to the gap is proportional to the function R that also appears in the number susceptibility,

$$\frac{\partial^2 p}{\partial \Delta^2} = -4M_D^2 R. \quad (72)$$

Consequently, from the above discussion of the eigenvalues $\tilde{\chi}_1, \tilde{\chi}_2$ we conclude

$$\frac{\partial^2 p}{\partial \Delta^2} < 0 \quad \Leftrightarrow \quad \tilde{\chi}_1, \tilde{\chi}_2 > 0. \quad (73)$$

C. Solutions to the gap equation

The stability analysis in the previous two subsections was performed without knowledge of the explicit solution of the gap equation: The screening masses are completely independent of the gap equation. For the number susceptibility, we made use of the gap equation in order to extract the derivative of the gap with respect to the two chemical potentials (which was done without solving the gap equation). Consequently, the main results of this paper, regions of (in)stability of the homogeneous phases and their connection to the regions of different Fermi surface topologies, do not need the explicit form of the gap function. However, one might say that not all regions of the phase diagram are accessible for solutions of the gap equation. Moreover, one would like to know which regions of the phase diagram are accessible to which coupling strengths. Therefore, in this subsection, we present the solution of the gap equation and its representation as lines in the phase diagram. We do so by first rewriting

the gap equation (50) in the above used dimensionless quantities,

$$-\kappa = K'_\rho(0, \infty) - K_\rho(\sqrt{\rho_-}, \sqrt{\rho_+}), \quad (74)$$

where

$$K'_\rho(0, \infty) \equiv \int_0^\infty dx \left[\frac{x^2}{\sqrt{(x^2 - \rho)^2 + 1}} - 1 \right], \quad (75a)$$

$$K_\rho(\sqrt{\rho_-}, \sqrt{\rho_+}) \equiv \int_{\sqrt{\rho_-}}^{\sqrt{\rho_+}} dx \frac{x^2}{\sqrt{(x^2 - \rho)^2 + 1}}. \quad (75b)$$

We have introduced the new dimensionless parameter

$$\kappa \equiv \frac{\pi}{2\sqrt{2m\Delta}a}, \quad (76)$$

which plays the role of the coupling strength: Small values, $\kappa \rightarrow -\infty$, correspond to the BCS limit, whereas large values, $\kappa \rightarrow +\infty$, correspond to the BEC limit. We solve Eq. (74) for a fixed κ to obtain ρ as a function of η . Let us explain this in somewhat more detail: After fixing κ , we first consider the region with no effective Fermi surface, i.e., we set $\rho_- = \rho_+ = 0$. In this case, the right-hand side of Eq. (74) does not depend on η , i.e., we obtain a constant number, say $\rho_0(\kappa)$, represented by a horizontal line in the phase diagram, see Fig. 5. Physically, this means that the average chemical potential does not change upon increasing the mismatch. This is true until the mismatch η reaches a critical value and the constant line reaches an area in the phase diagram with gapless excitations. Determined by the value $\rho_0(\kappa)$, this area can either be the region of one or of two effective Fermi surfaces. (Or it can be the “splitting point” shown in the middle of the figure, which is a special case that corresponds to the point “S” in the phase diagram in Ref. [21]. This point is hit by the line with $\kappa \simeq 0.84$). To obtain the continuation of the constant line, we switch on the terms ρ_+ (for one Fermi surface) or both ρ_- and ρ_+ (for two Fermi surfaces) in Eq. (74) and solve the equation from the point $\eta = \sqrt{\rho_0^2(\kappa) + 1}$ (for one Fermi surface) or $\eta = 1$ (for two Fermi surfaces). In Fig. 5 we show the solutions for four different coupling strengths, $\kappa = -1, 0, 1, 1.75$, two of which end up in the breached region for sufficiently large mismatches and two of which end up in the region with a single effective Fermi sphere. In particular, the line $\kappa = 0$, corresponding to the Feshbach resonance $a = \pm\infty$, hits the breached pair region. This is in agreement with previous mean-field studies.

All lines enter an unstable region for sufficiently large mismatches, meaning that an inhomogeneous phase, e.g., a LOFF or mixed phase, or the normal state take over. For all couplings κ that result in $\rho_0(\kappa) < 0$, the system passes, for mismatches $\eta > \sqrt{\rho_0^2(\kappa) + 1}$, through a stable gapless region with one effective Fermi surface and reaches, for even larger mismatches (η such that the left-hand side of Eq. (70) is smaller than zero), an unstable region.

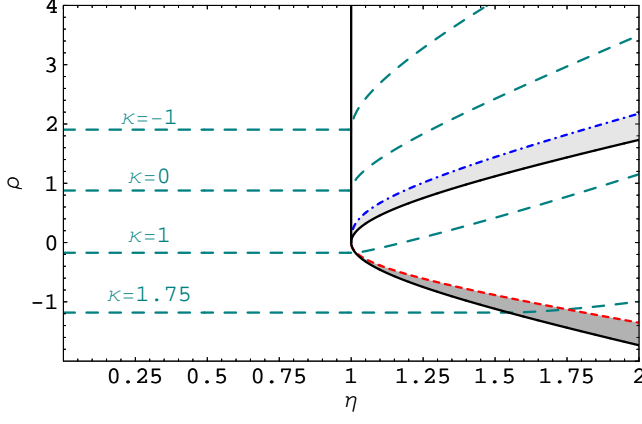


FIG. 5: (Color online) The solid lines are taken from Fig. 3. The dashed-dotted (blue online) and short-dashed (red online) curves as well as the shaded areas are taken from Fig. 4. The long-dashed (green online) curves are solutions of the gap equation for different coupling strengths κ .

VI. GENERALIZATION OF CLOGSTON LIMIT

So far we have investigated the stability of (gapless) superconductors with respect to a real magnetic screening mass and a positive number susceptibility. We have seen that the latter condition is equivalent to a local maximum of the pressure, Eq. (73). In this section, we ask which of the states in the phase diagram cannot be *global* maxima of the pressure. To this end, we compare the pressure in the superconducting state p_s with the one in the normal conducting state p_n and require the difference to be positive, $p_s - p_n > 0$. We do so for fixed chemical potentials. Therefore, p_n is the pressure of the vacuum in the case of negative chemical potentials. It is expected that the same analysis for fixed number densities leads to a different result.

The pressure in the normal phase is obtained by setting $\Delta = 0$ in Eq. (71),

$$\frac{p_n}{p_0} = \frac{\lambda^5}{5} - \rho \frac{\lambda^3}{3} + \frac{2}{15} [\Theta(\rho + \eta)(\rho + \eta)^{5/2} + \Theta(\rho - \eta)(\rho - \eta)^{5/2}], \quad (77)$$

where, in order to use the same dimensionless parameters as in the previous section, we introduced the gap Δ as the energy scale. Then, the pressure is given in units of

$$p_0 \equiv \frac{\sqrt{2} m^{3/2} \Delta^{5/2}}{\pi^2}, \quad (78)$$

and the cut-off Λ for the momentum integral in Eq. (71) is replaced by the dimensionless cut-off $\lambda \equiv \Lambda / \sqrt{2} m \Delta$. After writing the pressure p_s for the superconducting phase in dimensionless quantities, we find for the pressure dif-

ference the cut-off-independent expression

$$\begin{aligned} \Delta p \equiv \frac{p_s - p_n}{p_0} &= L'_\rho(0, \infty) - L_\rho(\sqrt{\rho_-}, \sqrt{\rho_+}) \\ &+ \frac{4}{15} \rho^{5/2} + \frac{\eta}{3} (\rho_+^{3/2} - \rho_-^{3/2}) \\ &- \frac{2}{15} [\Theta(\rho + \eta)(\rho + \eta)^{5/2} + \Theta(\rho - \eta)(\rho - \eta)^{5/2}]. \end{aligned} \quad (79)$$

Here we have, as in the previous sections, omitted the Θ -functions that come with ρ_+ and ρ_- , and we have abbreviated the integrals

$$L'_\rho(0, \infty) \equiv \int_0^\infty dx x^2 \left[\sqrt{(x^2 - \rho)^2 + 1} - \frac{1}{2\sqrt{(x^2 - \rho)^2 + 1}} - |x^2 - \rho| \right], \quad (80a)$$

$$L_\rho(\sqrt{\rho_-}, \sqrt{\rho_+}) \equiv \int_{\sqrt{\rho_-}}^{\sqrt{\rho_+}} dx x^2 \left[\sqrt{(x^2 - \rho)^2 + 1} - \frac{1}{2\sqrt{(x^2 - \rho)^2 + 1}} \right]. \quad (80b)$$

In Fig. 6 we show the solution to the equation $\Delta p = 0$, represented by the dashed-dotted (blue online) line. All states above (and right from) this line cannot be global maxima of the pressure because $\Delta p < 0$. We observe that the region excluded by this condition contains both the region of negative number susceptibility and imaginary Meissner mass. However, a gapless region with a single Fermi surface and $\Delta p > 0$ remains. Extending the results to larger mismatches than shown in the figure, $\eta > 2$, we find that the dashed and dashed-dotted lines approach each other, that is, for large η the stability conditions given by $\tilde{\chi}$ and Δp come to coincide.

The condition $\Delta p > 0$ excludes some fully gapped states. In particular, one may extend the results to large chemical potentials, corresponding to the weak coupling regime. One finds that the dashed-dotted line in Fig. 6 approaches a vertical line given by $\eta \simeq 1/\sqrt{2}$. That is no surprise, since here the original discussion by Clogston applies [36]. Analytically, in the weak coupling limit,

$$L'_\rho(0, \infty) \simeq \frac{\sqrt{\rho}}{4}. \quad (81)$$

Then, setting $\rho_- = \rho_+ = 0$ in Eq. (79) and expanding the expression for the pressure in the normal phase for $\rho \gg \eta$, we obtain

$$\Delta p \simeq \frac{\sqrt{\rho}}{2} \left(\frac{1}{2} - \eta^2 \right), \quad (82)$$

and we see that this expression is indeed negative for $\eta > 1/\sqrt{2}$.

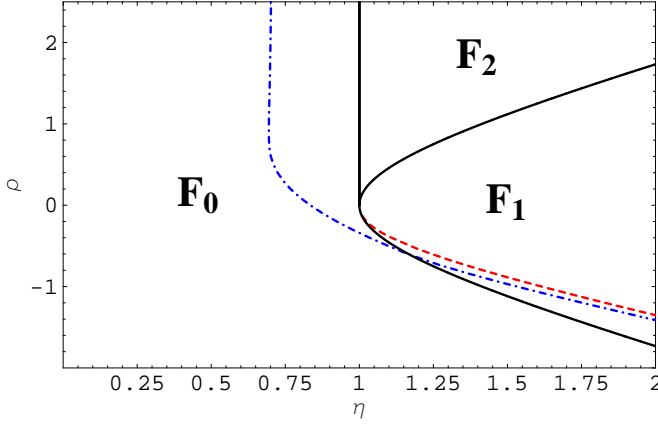


FIG. 6: (Color online) The solid lines are taken from Fig. 3. Dashed-dotted (blue online) line: Solution to $\Delta p = 0$. For all states above (below) this line, $\Delta p < 0$ ($\Delta p > 0$). For comparison, we also show the line given by the susceptibility condition (dashed, red online), see Fig. 4.

VII. STABILITY IN TWO DIMENSIONS

In this section, we re-do our stability calculations for $d = 2$ dimensional systems. This case has the advantage that the stability conditions can be discussed in forms of simple analytical expressions, as we show below. Apart from their theoretical convenience, one can certainly imagine performing experiments with quasi-two-dimensional superfluids/superconductors with mismatched Fermi surfaces.

We notice that Fig. 3 only depends on the form of the dispersion, $\epsilon_k \sim k^2$. Therefore, the boundaries of the regions F_0 , F_1 , and F_2 in this figure are valid also for two dimensions. The results for the Meissner mass and the number susceptibility, however, depend on the dimension. For $d = 2$ we use Eq. (43) and (53) – (55) with the following replacements. The elliptic integrals in Eqs. (34) become simple analytic expressions after reducing the powers of x in the numerator of the integrands by 1,

$$I_\rho^{2d}(a, b) = \frac{1}{2} \frac{x^2 - \rho}{\sqrt{(x^2 - \rho)^2 + 1}} \Big|_{x=a}^{x=b}, \quad (83a)$$

$$\tilde{I}_\rho^{2d}(a, b) = \frac{1}{2} \frac{\rho(x^2 - \rho) - 1}{\sqrt{(x^2 - \rho)^2 + 1}} \Big|_{x=a}^{x=b}. \quad (83b)$$

The integration boundaries do not depend on d , i.e., after evaluating the Θ -function, $\sqrt{\rho_+}$ and $\sqrt{\rho_-}$ appear as boundaries also in two dimensions. Again, the reason is that these quantities only depend on the dispersion, cf. Eq. (36). In the remaining terms, the powers of ρ_+ and ρ_- change. From Eqs. (35), (36), and the results in Appendix B, we conclude that in the expressions for the Meissner mass squared, $\rho_\pm^{3/2}$ has to be replaced by ρ_\pm . It should be mentioned that our definition for the Meissner mass cannot naively be transferred to two dimensions

(simply using a two-dimensional volume V in Eq. (18b) would not yield dimensions $[\text{energy}]^2$ for m_M^2). However, this is no problem for our stability analysis. The simplest way to think of the Meissner mass squared is as follows. In our model, the global number conservation group is spontaneously broken in the same way as the gauge group. Therefore, the Meissner mass squared is proportional to the number density of superfluid particles. The latter quantity has dimensions $[\text{energy}]^d$, i.e., it depends on the dimension d . Thus, although we are, strictly speaking, not discussing the Meissner mass in two dimensions, we can use the same stability condition (66) with the above replacements for $d = 2$ (and refer to it in the rest of this section as “stability with respect to the Meissner mass”). For the breached pair phase, Eq. (66) becomes

$$\frac{1}{2}(\rho + \sqrt{\rho^2 + 1}) - \frac{\rho\eta}{\sqrt{\eta^2 - 1}} = 0. \quad (84)$$

This equation has no solution in the relevant parameter range, i.e., for $\rho > \sqrt{\eta^2 - 1}$. The left-hand side is negative for all relevant η, ρ . Consequently, with respect to the Meissner mass, there is no stable breached pair state. For the case of a single effective Fermi sphere, this equation reads

$$\rho \left(1 - \frac{\eta}{\sqrt{\eta^2 - 1}} \right) = 0. \quad (85)$$

This equation is only solved by $\rho = 0$. Because the expression in parentheses is negative, states with $\rho > 0$ are unstable while states with $\rho < 0$ are stable with respect to the Meissner mass. As for $d = 3$ it is obvious that all fully gapped states are stable.

In the expression for the number susceptibility, $\sqrt{\rho_\pm}$ has to be replaced by $\rho_\pm^0 = 1$. For the breached pair state, the expressions for the eigenvalues of $\tilde{\chi}$ are, even for $d = 2$, too lengthy to show here. One checks numerically that at least one of the eigenvalues is negative. The phases with a single Fermi surface are treated with the same analysis as described in Sec. V B. Hence, we may use the two-dimensional analogue of Eq. (70) which is

$$1 - \frac{\eta}{\sqrt{\eta^2 - 1}} = 0. \quad (86)$$

This equation has no solution. Since the left-hand side is negative for any η , all states with a single Fermi sphere are unstable for $d = 2$.

We summarize these results in Fig. 7. This figure should be compared to its analogue in three dimensions, Fig. 4. We observe that both stability conditions are more restrictive in two dimensions. The condition of the positivity of the Meissner mass squared does not leave any stable breached pair phase. And the positivity of the number susceptibility does not leave any stable phase with one effective Fermi surface. Again, the unstable region with respect to the Meissner mass is a subset of the

unstable region with respect to the number susceptibility. So the stable regions are determined solely by the number susceptibility. Unlike in the case $d = 3$, the lines that separate stable from unstable regions are exactly on top of lines that separate different Fermi surface topologies. In some recent papers general connections between stability and Fermi surface topology have been proposed [37, 38]. General results for topological stability are obtained using K-theory [37] and are given in terms of the dimensionality of the system and of the effective Fermi surface. It would be interesting to see if similar analyses apply to the situations considered in this paper.

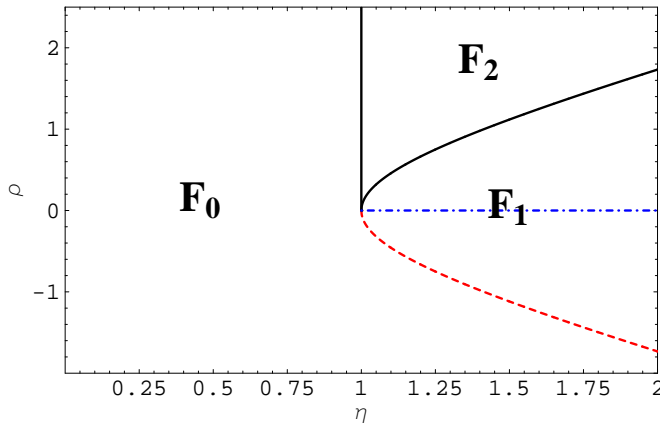


FIG. 7: (Color online) Unstable regions in two-dimensional systems. The region between the solid vertical and the dashed (red online) lines is unstable with respect to the number susceptibility. The region between the solid vertical and the dashed-dotted (blue online) lines is unstable with respect to the Meissner mass. The dashed line exactly coincides with the line that separates fully gapped phases from phases with one effective Fermi surface.

VIII. CONCLUSIONS

We have studied stability conditions and their relation to different Fermi surface topologies in a superconductor of two fermion species with mismatched chemical potentials. The results have been presented in a phase diagram in which the mismatch and the average chemical potential serve as parameters. Determining the zeroes of one of the two quasiparticle excitation energies provides lines in the phase diagram that separate regions with zero, one and two effective Fermi spheres (these lines are given by simple analytic expressions). We have computed the Meissner mass (squared) and the number susceptibility matrices. Both of these 2×2 matrices have to be positive definite in a stable state. Consequently, they define lines in the phase diagram separating stable from unstable phases with respect to these conditions. Up to remaining elliptic integrals, we have derived analytic expressions for these lines. The two expressions are amazingly similar.

Moreover they are close to, but not identical with, the lines that separate phases with different Fermi surface topologies. We have found that the condition with respect to a real Meissner mass leaves a stable breached pair phase. However, this region is rendered unstable by a negative eigenvalue of the number susceptibility matrix. Stable gapless states with a single Fermi surface exist for negative average chemical potentials. Solution of the gap equation shows that these states are on the BEC side of the Feshbach resonance.

Comparing local and global stability conditions, we have identified possible regions of metastability. That possibility seems particularly interesting from an experimental point of view, because the onset of catastrophic and practically unpredictable (nucleated) decay, as a function of coupling constant or number density, would be a striking physical phenomenon.

Our results suggest several future studies. Interesting theoretical questions are related to the apparent connection of the stability conditions with the Fermi surface topology. Is there a qualitative reason why the stability lines lie very close to, but do not coincide with, the lines marking topology change? Is there a qualitative reason why phases with a single Fermi sphere are stable (at least in a certain region of the phase diagram), but phases with two effective Fermi spheres are unstable? From the experimental point of view, it remains challenging to define practically accessible signatures of the gapless phases. Our calculation of the screening masses could be used to predict transport properties of atomic gapless superfluids.

Acknowledgments

The authors thank M. Alford, A. Chitov, M. Mannarelli, E. Mishchenko, I. Shovkovy, and M. Zwierlein for valuable comments and discussions. AS acknowledges support by the German Academic Exchange Service (DAAD) and the U.S. Department of Energy under contracts DE-FG02-91ER50628 and DE-FG01-04ER0225 (OJI). FW acknowledges support from the U. S. Department of Energy contract DE-FG02-05ER41360.

APPENDIX A: MATSUBARA SUMS FOR THE SCREENING MASSES

In this appendix, we explain how to obtain the expressions (30) and (31) from the definitions (18). In particular, this calculation includes the summation over fermionic Matsubara frequencies. For the Debye and Meissner masses we need to compute the following quan-

tities,

$$\begin{aligned} M_a &\equiv T \sum_n \text{Tr}[S(K)\bar{\Gamma}_a^2] \\ &= g_a^2 T \sum_n \text{Tr}[G^+(K)T_a - G^-(K)T_a], \quad (\text{A1}) \end{aligned}$$

and

$$\begin{aligned} N_{ab}^\pm &\equiv T \sum_n \text{Tr}[S(K)\Gamma_a^\pm S(K-P)\Gamma_b^\pm] \\ &= g_a g_b T \sum_n \text{Tr}[G^+(K)T_a G^+(K-P)T_b \\ &\quad + G^-(K)T_a G^-(K-P)T_b] \\ &\quad \pm T \sum_n \text{Tr}[F^-(K)T_a F^+(K-P)T_b \\ &\quad + F^+(K)T_a F^-(K-P)T_b], \quad (\text{A2}) \end{aligned}$$

where the trace over Nambu-Gorkov space has been performed. In order to compute M_{ab} , we insert the normal

and anomalous propagators from Eq. (11) into Eq. (A1) and perform the trace over two-fermion space. In this case, the Matsubara sum can be easily performed. We set the gauge boson energy to zero, $p_0 = 0$ and take the zero-temperature limit (where we assume, without loss of generality, $\mu_1 > \mu_2$ and hence $\delta\mu > 0$). Hereafter, we take the limit of a vanishing gauge boson momentum, $\mathbf{p} \rightarrow 0$ and obtain

$$\frac{M_{1/2}}{g_{1/2}^2} = \pm \frac{\epsilon_k \pm \xi_k}{\epsilon_k} \Theta(\delta\mu - \epsilon_k) - \frac{\xi_k}{\epsilon_k}. \quad (\text{A3})$$

In order to compute N_{ab}^\pm , we insert the fermion propagators into Eq. (A2). In this case, the Matsubara sums are more complicated. We make use of the following two generic formulas, which can be derived via contour integration in the complex k_0 -plane. For real numbers $\alpha, \beta, \delta_1, \delta_2, a > 0, b > 0$, we have

$$\begin{aligned} &T \sum_n \frac{(k_0 + \alpha)(k_0 - p_0 + \beta)}{[(k_0 \pm \delta_1)^2 - a^2][(k_0 - p_0 \pm \delta_2)^2 - b^2]} \\ &= \frac{1}{4ab} \left\{ \frac{(a_\mp + \alpha)(b_\pm - \beta)}{p_0 - a_\mp - b_\pm} [1 - n(a_\mp) - n(b_\pm)] - \frac{(a_\pm - \alpha)(b_\mp + \beta)}{p_0 + a_\pm + b_\mp} [1 - n(a_\pm) - n(b_\mp)] \right. \\ &\quad \left. + \frac{(a_\pm - \alpha)(b_\pm - \beta)}{p_0 + a_\pm - b_\pm} [n(a_\pm) - n(b_\pm)] - \frac{(a_\mp + \alpha)(b_\mp + \beta)}{p_0 - a_\mp + b_\mp} [n(a_\mp) - n(b_\mp)] \right\} \quad (\text{A4}) \end{aligned}$$

where $k_0 = -i(2n+1)\pi T$ and $p_0 = -i2m\pi T$ are the fermionic and bosonic Matsubara frequencies, respectively, and $n(x) \equiv 1/(\exp(x/T) + 1)$ is the Fermi distribution. Moreover, $a_\pm \equiv a \pm \delta_1, b_\pm \equiv b \pm \delta_2$. And

$$\begin{aligned} &T \sum_n \frac{1}{[(k_0 \pm \delta_1)^2 - a^2][(k_0 - p_0 \pm \delta_2)^2 - b^2]} \\ &= \frac{1}{4ab} \left\{ \frac{1}{p_0 + a_\pm + b_\mp} [1 - n(a_\pm) - n(b_\mp)] - \frac{1}{p_0 - a_\mp - b_\pm} [1 - n(a_\mp) - n(b_\pm)] \right. \\ &\quad \left. + \frac{1}{p_0 + a_\pm - b_\pm} [n(a_\pm) - n(b_\pm)] - \frac{1}{p_0 - a_\mp + b_\mp} [n(a_\mp) - n(b_\mp)] \right\}. \quad (\text{A5}) \end{aligned}$$

After applying these results, we again set $p_0 = 0$ and take the limits $T \rightarrow 0, \mathbf{p} \rightarrow 0$. We obtain

$$\frac{N_{11}^\pm}{g_1^2} = -\frac{\Delta^2}{2\epsilon_k^3} \Theta(\epsilon_k - \delta\mu) - \frac{(\epsilon_k + \xi_k)^2}{2\epsilon_k^2} \delta(\epsilon_k - \delta\mu), \quad (\text{A6a})$$

$$\frac{N_{22}^\pm}{g_2^2} = -\frac{\Delta^2}{2\epsilon_k^3} \Theta(\epsilon_k - \delta\mu) - \frac{(\epsilon_k - \xi_k)^2}{2\epsilon_k^2} \delta(\epsilon_k - \delta\mu), \quad (\text{A6b})$$

$$\begin{aligned} \frac{N_{12}^\pm}{g_1 g_2} &= \frac{N_{21}^\pm}{g_1 g_2} \\ &= \pm \left[\frac{\Delta^2}{2\epsilon_k^3} \Theta(\epsilon_k - \delta\mu) - \frac{\Delta^2}{2\epsilon_k^2} \delta(\epsilon_k - \delta\mu) \right]. \quad (\text{A6c}) \end{aligned}$$

Inserting Eqs. (A3) and (A6) into (18) yields (30) and (31).

APPENDIX B: INTEGRALS IN MEISSNER MASS

Here we derive the Meissner mass, Eq. (43), from Eqs. (31). With

$$J_\rho^\pm(a, b) \equiv \int_a^b dx x^2 \left(1 \pm \frac{x^2 - \rho}{\sqrt{(x^2 - \rho)^2 + 1}} \right) \quad (\text{B1})$$

$$\begin{aligned} \frac{m_{M,11/22}^2}{g_{1/2}^2 M_M^2} = & 3 \left[J_\rho^-(0, \infty) \pm J_\rho^\pm(\sqrt{\rho_-}, \sqrt{\rho_+}) \right] - \left[\tilde{I}_\rho(0, \infty) - \tilde{I}_\rho(\sqrt{\rho_-}, \sqrt{\rho_+}) \right] \\ & - \left[\frac{(\eta \pm \sqrt{\eta^2 - 1})^2}{2\eta\sqrt{\eta^2 - 1}} \rho_+^{3/2} + \frac{(\eta \mp \sqrt{\eta^2 - 1})^2}{2\eta\sqrt{\eta^2 - 1}} \rho_-^{3/2} \right], \end{aligned} \quad (\text{B2a})$$

$$\frac{m_{M,12}^2}{g_1 g_2 M_M^2} = \frac{m_{M,21}^2}{g_1 g_2 M_M^2} = \tilde{I}_\rho(0, \infty) - \tilde{I}_\rho(\sqrt{\rho_-}, \sqrt{\rho_+}) - \frac{\rho_+^{3/2} + \rho_-^{3/2}}{2\eta\sqrt{\eta^2 - 1}}. \quad (\text{B2b})$$

The result for the diagonal elements $m_{M,11/22}^2$ is simplified by observing that the integrals J_ρ^\pm and \tilde{I}_ρ are in fact related via partial integration,

$$J_\rho^\pm(a, b) = \frac{b^3}{3} \left(1 \pm \frac{b^2 - \rho}{\sqrt{(b^2 - \rho)^2 + 1}} \right) - \frac{a^3}{3} \left(1 \pm \frac{a^2 - \rho}{\sqrt{(a^2 - \rho)^2 + 1}} \right) \mp \frac{2}{3} \tilde{I}_\rho(a, b). \quad (\text{B3})$$

In particular,

$$J_\rho^-(0, \infty) = \frac{2}{3} \tilde{I}_\rho(0, \infty). \quad (\text{B4})$$

Rewriting $J_\rho^-(0, \infty)$ and $J_\rho^\pm(\sqrt{\rho_-}, \sqrt{\rho_+})$ in Eq. (B2a) with the help of these relations renders the diagonal el-

and the integral $\tilde{I}_\rho(a, b)$ defined in Eq. (34b), we obtain from Eqs. (31)

ements identical to the off-diagonal ones, and we arrive at Eq. (43).

-
- [1] J. Bardeen, L.N. Cooper, and J.R. Schrieffer, Phys. Rev. **108**, 1175 (1957).
 - [2] A.J. Leggett, Rev. Mod. Phys. **47**, 331 (1975); D. Vollhardt and P. Wölfle, *The Superfluid Phases of Helium 3* (Taylor & Francis, London, 1990).
 - [3] J.G. Bednorz and K.A. Müller, Z. Physik B **64**, 189 (1986); M. Sigrist and K. Ueda, Rev. Mod. Phys. **63**, 239 (1991).
 - [4] T. Schäfer, Phys. Rev. D **62**, 094007 (2000) [arXiv:hep-ph/0006034]; A. Schmitt, Phys. Rev. D **71**, 054016 (2005) [arXiv:nucl-th/0412033].
 - [5] C.-H. Pao, S.-T. Wu, S.-K. Yip, arXiv:cond-mat/0506437.
 - [6] E. Gubankova, W. V. Liu and F. Wilczek, Phys. Rev. Lett. **91**, 032001 (2003) [arXiv:hep-ph/0304016].
 - [7] W. V. Liu and F. Wilczek, Phys. Rev. Lett. **90**, 047002 (2003) [arXiv:cond-mat/0208052].
 - [8] E. Gubankova, F. Wilczek and E. G. Mishchenko, Phys. Rev. Lett. **94**, 110402 (2005) [arXiv:cond-mat/0409088].
 - [9] C.A. Regal, M. Greiner, and D.S. Jin, Phys. Rev. Lett. **92**, 040403 (2004) [arXiv:cond-mat/0401554]; M. Bartenstein *et al.*, Phys. Rev. Lett. **92**, 120401 (2004) [arXiv:cond-mat/0401109]; M.W. Zwierlein *et al.*, Phys. Rev. Lett. **92**, 120403 (2004) [arXiv:cond-mat/0403049]; J. Kinast *et al.*, Phys. Rev. Lett. **92**, 150402 (2004) [arXiv:cond-mat/0403540]; T. Bourdel *et al.*, Phys. Rev. Lett. **93**, 050401 (2004) [arXiv:cond-mat/0403091].
 - [10] P. Noziers and S. Schmitt-Rink, J. Low. Temp. Phys. **59**, 195 (1985); M. Marini, F. Pistolesi, and G.C. Strinati, Eur. J. Phys. B **1**, 151 (1998) [arXiv:cond-mat/9703160]; E. Babaev, Phys. Rev. B **63**, 184514 (2001) [arXiv:cond-mat/0010085].
 - [11] M. W. Zwierlein, A. Schirotzek, C. H. Schunck and W. Ketterle, Science **311**, 492 (2006) [arXiv:cond-mat/0511197].
 - [12] G. B. Partridge, W. Li, R. I. Kamar, Y. Liao

- and R. G. Hulet, *Science* **311**, 503 (2006) [arXiv:cond-mat/0511752].
- [13] P. F. Bedaque, H. Caldas and G. Rupak, *Phys. Rev. Lett.* **91**, 247002 (2003) [arXiv:cond-mat/0306694]; M. M. Forbes, E. Gubankova, W. V. Liu and F. Wilczek, *Phys. Rev. Lett.* **94**, 017001 (2005) [arXiv:hep-ph/0405059]; J. Carlson and S. Reddy, *Phys. Rev. Lett.* **95**, 060401 (2005) [arXiv:cond-mat/0503256].
- [14] D. Bailin and A. Love, *Phys. Rept.* **107**, 325 (1984).
- [15] For reviews, see K. Rajagopal and F. Wilczek, arXiv:hep-ph/0011333; M. G. Alford, *Ann. Rev. Nucl. Part. Sci.* **51**, 131 (2001) [arXiv:hep-ph/0102047]; D. H. Rischke, *Prog. Part. Nucl. Phys.* **52**, 197 (2004) [arXiv:nucl-th/0305030]; I. A. Shovkovy, *Found. Phys.* **35**, 1309 (2005) [arXiv:nucl-th/0410091].
- [16] M. G. Alford, K. Rajagopal and F. Wilczek, *Nucl. Phys. B* **537**, 443 (1999) [arXiv:hep-ph/9804403].
- [17] K. Rajagopal and A. Schmitt, *Phys. Rev. D* **73**, 045003 (2006) [arXiv:hep-ph/0512043].
- [18] M. Kitazawa, D. H. Rischke and I. A. Shovkovy, arXiv:hep-ph/0602065.
- [19] M. Huang and I. A. Shovkovy, *Phys. Rev. D* **70**, 094030 (2004) [arXiv:hep-ph/0408268].
- [20] R. Casalbuoni, R. Gatto, M. Mannarelli, G. Nardulli and M. Ruggieri, *Phys. Lett. B* **605**, 362 (2005) [Erratum-ibid. B **615**, 297 (2005)] [arXiv:hep-ph/0410401]; K. Fukushima, *Phys. Rev. D* **72**, 074002 (2005) [arXiv:hep-ph/0506080].
- [21] D. T. Son and M. A. Stephanov, arXiv:cond-mat/0507586.
- [22] A. I. Larkin and Yu. N. Ovchinnikov, *Zh. Eksp. Teor. Fiz.* **47**, 1136 (1964) [*Sov. Phys. JETP* **20**, 762 (1965)]; P. Fulde and R. A. Ferrell, *Phys. Rev.* **135**, A550 (1964).
- [23] M. G. Alford, J. A. Bowers and K. Rajagopal, *Phys. Rev. D* **63**, 074016 (2001) [arXiv:hep-ph/0008208]; I. Giannakis and H. C. Ren, *Phys. Lett. B* **611**, 137 (2005) [arXiv:hep-ph/0412015].
- [24] D.E. Sheehy and L. Radzihovsky, *Phys. Rev. Lett.* **96**, 060401 (2006) [arXiv:cond-mat/0508430].
- [25] L. He, M. Jin and P. f. Zhuang, arXiv:cond-mat/0601147.
- [26] A. Bulgac, M. McNeil Forbes and A. Schwenk, arXiv:cond-mat/0602274.
- [27] J.M. Cornwall, R. Jackiw, and E. Tomboulis, *Phys. Rev. D* **10**, 2428 (1974).
- [28] J.I. Kapusta, *Finite-temperature field theory* (Cambridge University Press, Cambridge, 1989).
- [29] I. Shovkovy and M. Huang, *Phys. Lett. B* **564**, 205 (2003) [arXiv:hep-ph/0302142].
- [30] L. n. He, M. Jin and P. f. Zhuang, *Phys. Rev. B* **73**, 024511 (2005) [arXiv:hep-ph/0509317].
- [31] E. V. Gorbar, M. Hashimoto, V. A. Miransky and I. A. Shovkovy, arXiv:hep-ph/0602251.
- [32] S.-T. Wu and S.-K. Yip, *Phys. Rev. A* **67**, 053603 (2003) [arXiv:cond-mat/0303185].
- [33] L. n. He, M. Jin and P. f. Zhuang, arXiv:cond-mat/0604137.
- [34] A. Schmitt, Q. Wang and D. H. Rischke, *Phys. Rev. D* **69**, 094017 (2004) [arXiv:nucl-th/0311006].
- [35] M. Mannarelli, G. Nardulli and M. Ruggieri, arXiv:cond-mat/0604579.
- [36] A.M. Clogston, *Phys. Rev. Lett.* **9**, 266 (1962); B.S. Chandrasekhar, *Appl. Phys. Lett.* **1**, 7 (1962).
- [37] P. Horava, *Phys. Rev. Lett.* **95**, 016404 (2005) [arXiv:hep-th/0503006].
- [38] G. E. Volovik, arXiv:cond-mat/0601372.